Catalysis Today 172 (2011) 103–110

Contents lists available at ScienceDirect

Catalysis Today

journal homepage: www.elsevier.com/locate/cattod

Hydrogenolysis of anisole over mesoporous sulfided CoMoW/SBA-15(16) catalysts

C.V. Loricera[a], B. Pawelec[a,*], A. Infantes-Molina[a,*], M.C. Álvarez-Galván[a], R. Huirache-Acuña[b], R. Nava[c], J.L.G. Fierro[a]

[a] Instituto de Catálisis y Petroleoquímica, CSIC, c/Marie Curie, 2, Cantoblanco, 28049 Madrid, Spain
[b] Facultad de Ingeniería Química, Universidad Michoacana de San Nicolás de Hidalgo, 58060 Morelia, Michoacán, Mexico
[c] Universidad Autónoma de Querétaro (UAQ), 76000 Querétaro, Mexico

ARTICLE INFO

Article history:
Received 30 November 2010
Received in revised form 14 February 2011
Accepted 15 February 2011
Available online 1 April 2011

Keywords:
SBA-15
SBA-16
Cobalt–molybdenum–tungsten
Hydrodeoxygenation
Anisole
Phosphate
Hydrotreatment

ABSTRACT

This contribution describes the effect of SBA-15(16) support modification with variable quantity of P_2O_5 (0.5 and 1.0 wt%) on the catalytic response of supported ternary CoMoW catalysts tested in the gas-phase hydrogenolysis of anisole, as a model compound for pyrolysis oil. The catalysts were characterized by a variety of techniques (S_{BET}, XRD, TPD-NH_3, XPS, HRTEM and coke combustion followed by TG/DTG). Under steady-state conditions, the sulfided CoMoW/SBA-16 catalyst modified with a small amount of phosphate (0.5 wt%) recorded the highest activity and stability in anisole transformation at 310 °C and 3 MPa of hydrogen pressure. All catalysts exhibited similar selectivities at the same anisole conversion (38%), indicating that catalyst morphology did not influence the catalytic behavior. Regardless of the carrier, deoxygenation was not significant, with demethylation (phenol) and isomerization (*o*-cresol, *o*-xylenol) being the main reaction routes. The highest activity recorded by the phosphate-containing CoMoW/SBA-16 catalyst is associated with its highest total acidity, the largest population of Mo(W)S_2 phases located mainly within the inner support porous structure, the greatest sulfidation degree of W species and major stability during time-on-stream operation with respect to other catalysts.

1. Introduction

Nowadays, there is considerable interest in developing alternative materials for fuel production from bio-liquids [1,2]. Liquefied biomass can be used as a refinery feed, or it could be mixed with traditional feedstock after first removing of any oxygen-containing compounds. Removing oxygen from bio-liquids is an obligatory process because high oxygen content contributes to high viscosity, non-volatility, poor heating value, corrosiveness, immiscibility with fossil fuels, thermal instability and a tendency to polymerization during storage and transportation [3]. Thus, the total or partial removal of oxygenates from bio-liquids is required [4]. Accordingly, removing oxygen from bio-oils via hydrotreatment over conventional sulfided Co(Ni)Mo/Al_2O_3 catalysts allows using the existing petroleum refining infrastructure [2 and references within]. However, such catalysts were found to quickly deactivate by coke deposition because of the acidity of the reactants [5]. The challenge is therefore to design new bifunctional catalysts capable of maintaining stability during the on-stream conditions of bio-oil hydrotreatment.

Due to the highly complex composition of any bio-liquid [4,6], it is common practice to test new catalytic systems in the HDO of model compounds [5,7–15]. Among O-containing model compounds, anisole is the one less studied [11–15], even though its structure is similar to the main products of lignin depolymerisation during the fast pyrolysis of wood. A very early study by Huuska et al. [13] showed that bifunctional (acid and metal) catalysts are needed for the hydrogenolysis and hydrocracking of the carbon–oxygen bond of anisole, but also that catalyst acidity should be optimized because of the large decrease in anisole conversion due to coke formation on standard CoMo catalysts, in close agreement with our previous observations on hydrotreating catalysts [16].

The selection of catalysts for the HDO of bio-liquids depends heavily on both feedstock and operating conditions, with sulfided CoMo/Al_2O_3 catalysts being the preferred option in a hydrotreating reaction at low hydrogen pressure and high space velocities [17]. A recent study has revealed that metallic-like so-called brim sites, not sulfur anion vacancies (CUS sites), are involved in the hydrogenation reactions on sulfided CoMo catalysts, with the support interactions being responsible for the change both in the tendency to form vacancies and in the properties of the brim sites [17–19].

* Corresponding author.
E-mail addresses: bgarcia@icp.csic.es (B. Pawelec), ainfantes@icp.csic.es (A. Infantes-Molina).

0920-5861/$ – see front matter © 2011 Elsevier B.V. All rights reserved.
doi:10.1016/j.cattod.2011.02.037

Indeed, it is well known that Type II MoS_2-based structures, with only weak interactions with the support, have a higher catalytic activity than Type I MoS_2-based structures, where Mo–O linkages to the alumina are present [18]. Brønsted acid centers associated with Mo atoms together with the SH^- groups (involved in providing Brønsted acid sites and in the supply of hydrogen) were proposed as hydrogenolysis sites [20,21].

In order to substitute the standard alumina support, metal sulfides supported on neutral materials such as carbon, silica, alumina modified by K and mesoporous silicas for the HDO reaction have been studied [6–9]. Compared with silica, the mesoporous silica SBA-15 and SBA-16 materials have the advantages of high surface-to-volume ratio, variable framework compositions and high thermal stability. Indeed, our recent study on bio-liquid upgrading over sulfide CoMo supported on different mesoporous silicas (SBA-15, SBA-16, HMS and DMS-1) showed that those catalysts are effective in the hydrotreating of bio-liquid [6]. Moreover, support morphology was found to affect the distribution of products, with CoMo/SBA-16 catalyst being the most selective toward O-free products [6]. This finding suggests that the SBA-16 substrate with a 3D cubic arrangement of mesopores corresponding to *Im*3*m* space group symmetry [22] could be more effective as support than SBA-15 with hexagonal pores in a 2D array of long 1D channels (P6*mm* plane group) [23].

This study seeks to determine the factors influencing anisole transformation over sulfided Co–Mo–W catalysts supported on SBA-15 and SBA-16 materials. In particular, we are interested to see whether activity and selectivity are impacted by a decrease in support interaction by decorating the surface of SBA-15 and SBA-16 materials with P_2O_5 clusters. Factors influencing on the catalyst deactivation have been discussed.

2. Experimental

2.1. Synthesis of SBA-15 and SBA-16 supports and supported CoMoW catalysts

The siliceous SBA-15 and SBA-16 mesoporous substrates were synthesized according to the procedure described by Flodström and Alfredsson [24]. Triblock copolymers Pluronic P123 ($EO_{20}PO_{70}EO_{20}$, BASF) and F127 ($EO_{106}PO_{70}EO_{106}$, BASF) were used as surfactants in order to organize silica into highly ordered 2D hexagonal (SBA-15) and 3D cubic (SBA-16) structures, respectively. In a typical synthesis, the template was dissolved in an aqueous solution of HCl 4 M under stirring, after which the required amount of tetraethyl orthosilicate, as a source of silica (TEOS, 98%, Aldrich), was added to the solution at 25 °C and kept under stirring conditions for 24 h. The mixture was subsequently transferred into polypropylene bottles and heated at 80 °C for 24 h. The solid obtained was then filtered, washed thoroughly with deionized water and dried at 110 °C for 18 h. The organic template was removed by calcination at 500 °C for 6 h. Finally, the phosphate-modified materials were prepared via incipient wetness impregnation of SBA-15(16) substrates with aqueous solutions of H_3PO_4 of appropriate concentration to obtain substrates with P_2O_5 loadings of 0.5 and 1.0 wt%. After water evaporation at room temperature, the solid was dried at 110 °C for 4 h and then calcined at 500 °C for 4 h.

Two series of CoMoW catalysts were prepared using the SBA-15- and SBA-16-based substrates. The catalysts were prepared by simultaneous impregnation following the incipient wetness method using an aqueous solution containing ammonium heptamolybdate tetrahydrate ($(NH_4)_6Mo_7O_{24}{\cdot}4H_2O$, Aldrich), ammonium metatungstate ($(NH_4)_6H_2W_{12}O_{40}{\cdot}xH_2O$, Aldrich) and cobalt nitrate hexahydrate ($Co(NO_3)_2{\cdot}6H_2O$, Aldrich, 98%). Each support was loaded with fixed amounts of Mo (8.53 wt% of MoO_3), W (13.5 wt% of WO_3) and Co (3.81 wt% of CoO). The concentrations were calculated to provide a Mo/W atomic ratio of 0.5 and a Co/Mo atomic ratio of 0.3. Depending on the phosphate content (0.5 or 1.0 wt%), the catalysts will be named hereafter as 0.0P-S15(16), 0.5P-S15(16) and 1.0P-S15(16), where S15 and S16 are SBA-15 and SBA-16 materials, respectively.

2.2. Characterization techniques

BET specific surface areas were obtained from nitrogen adsorption–desorption measured at −196 °C on a Micromeritics TriStar 3000 apparatus with all sulfided samples outgassed at 270 °C for 5 h prior to analysis. Pore size distributions were analyzed by the BJH method. The pure supports and sulfided catalysts were characterized by powder X-ray diffractometry according to the step-scanning procedure (step size 0.02°; 0.5 s) with a computerized Seifert 3000 diffractometer, using Ni-filtered CuKα ($\lambda = 0.15406$ nm) radiation and a PW 2200 Bragg-Brentano $\theta/2\theta$ goniometer equipped with a bent graphite monochromator and an automatic slit. The acidity of the oxide precursors was determined by temperature-programmed desorption (TPD) of ammonia measurements, carried out in a Micromeritics TPR/TPD 2900 instrument. Infrared spectra of NO adsorption on sulfided catalysts were recorded in the diffuse reflectance mode on a FTIR-6300 JASCO Fourier transform spectrophotometer equipped with a Harrick diffuse reflectance accessory (HVC-DRP cell). The spent catalysts were studied by HRTEM microscopy using a JEM 2100F microscope operating with a 200 kV accelerating voltage and fitted with an INCA X-sight (Oxford Instruments). X-ray photoelectron spectra (XPS) of the spent catalysts were performed on a VG Escalab 200R spectrometer equipped with a hemispherical electron analyzer using a Mg Kα ($h\nu = 1253.6$ eV) X-ray source. The procedure followed during XPS measurements has been described elsewhere [25]. The amount of coke in the spent catalysts was determined with thermogravimetric TGA/SDTA851 equipment (Mettler Toledo) by measuring the weight change in the coked catalysts during the oxidation of spent catalysts. Coke was burnt by raising the sample temperature from r.t. to a final temperature of 900 °C at a rate of 10 °C min^{-1} in a 20%/80% O_2/N_2 mixture.

2.3. Catalytic activity measurements

The hydroconversion of the anisole was performed in a high-pressure laboratory-scale set-up equipped with a down-flow fixed bed catalytic reactor. Each experiment used 0.1 g of catalyst (particle diameter: 0.25–0.30 mm) mixed with 0.30 g of SiC (diameter 0.5 mm). Before catalyst activation, the catalyst was dried under a N_2 flow of 100 mL min^{-1} at 150 °C for 0.5 h. The catalyst was then sulfided in situ at 400 °C for 4 h at atmospheric pressure by a mixture of 10 vol% of a H_2S:H_2. After sulfidation, the catalyst was purged under a N_2 flow of 100 mL min^{-1} at 400 °C for 0.5 h and then stored overnight under a N_2 flow. Before the experimental run, the N_2 pressure was increased to the desired value (3.0 MPa), and the catalytic bed was cooled down to the temperature of the HDO reaction (310 °C). After that, N_2 flow was shut down, the liquid feed (20 vol% of anisole dissolved in hexadecane) injected by a high-pressure HPLC Knauer pump (WHSV = 24.5 h^{-1}) into a hydrogen stream was fed to the preheated reactor. Owing to the high boiling point of the reactant and the solvent, on-line analysis of the reaction products was not convenient. Consequently, the reactor effluents were condensed, and liquid samples were analyzed by a GC Agilent 6890A with a FID detector.

Activity at steady-state conditions is described in terms of the specific reaction rate according to Eq. (1):

$$r = \frac{X \cdot F}{m} \quad (1)$$

where r is the specific rate ($mol_{anisole}\ g_{cat}^{-1}\ s^{-1}$), X is the conversion of anisole, F is the molar flow rate of this reactant ($mol\ s^{-1}$), and m refers to the catalyst weight (g). Catalyst deactivation was calculated from the equation:

$$\frac{(X_{1h} - X_{4h}) \times 100\%}{X_{1h}} \quad (2)$$

3. Results and discussion

3.1. Characterization of supports and oxide precursors

The formation of hexagonal 2D and 3D cubic arrangements of SBA-15 and SBA-16 supports, respectively, were confirmed by a low-angle XRD technique (XRD patterns not shown here). Thus, the XRD patterns of all SBA-15-based supports showed three well-resolved typical diffraction peaks associated with a bi-dimensional *p6mm* hexagonal symmetry: one high-intensity peak at about $2\theta = 1.0^\circ$ (1 0 0) and two low-intensity peaks at about $2\theta = 1.7$ and 2.0° corresponding to (1 1 0) and (2 0 0) reflections, respectively. Similarly, the pure SBA-16 material had three peaks corresponding to the XRD reflection indexes of (1 1 0), (2 0 0) and (2 1 1), indicating that this substrate has a 3D cubic arrangement of mesopores corresponding to *Im3m* space group symmetry. As expected, the post-synthetic modification of the SBA-15(16) surfaces with H_3PO_4 did not change the support structure and pore arrangement was maintained throughout 4 h of reaction time, as confirmed by the HRTEM technique for spent catalysts.

Temperature-programmed desorption of ammonia (TPD-NH_3) was carried out in order to compare the acidity of oxide precursors. After Gaussian deconvolution of the TPD-NH_3 profiles (not shown here), the peaks corresponding to weak, medium and strong acid sites were obtained. The number of corresponding acid sites, expressed as mmol of ammonia per gram of catalyst, is compiled in Table 1. As seen in this table, the total acidity of the oxide precursors follows the trend: 0.5P-S16 > 0.0P-S15(16) > 1.0P-S15(16) ≈ 0.5P-S15. Thus, both P-free catalysts have the same number of acid sites. Since the formation of multiple bonding between the SBA-15(16) substrate and phosphoric acid depends on the degree of hydration of the support and the concentration of phosphoric acid [26], the number of medium and strong acid sites of the 0.5P-S16 sample apparently increased with respect to P-free material. This increase in acidity is probably due to the formation of $P(OH)_2$–O–Si bonds or even to free $OP(OH)_3$ entities interacting with the SBA-16 surface via H-bonding, as it was discussed by Stanislaus et al. [26]. Indeed, our DRIFTS spectroscopy results (data not show here) confirmed the formation of Brønsted acid sites after SBA-15(16) support modification with phosphate. With the exception of the 0.5P-S16 substrate, the presence of phosphate species on the surfaces of SBA-15 and SBA-16 materials led to a decrease in overall acidity, in good agreement with Stanislaus et al. [26]. The decrease in total acidity with an increase in phosphate content could also be explained by considering that during co-impregnation there is a higher preference of Mo(W) ions for P–OH groups than of cobalt ones [27]. Accordingly, the reaction of Mo(W) ions with phosphate anions led to the formation of phosphomolybdic (phosphotungstic) acid and/or phosphomolybdates (phosphotungstates), which are decomposed during calcination and form $Mo(W)O_3$ species adsorbed on basic sites, whereas the phosphate ions are adsorbed on more acidic sites [28].

3.2. Characterization of sulfided catalysts

The textural properties of sulfided catalysts were evaluated by nitrogen adsorption–desorption isotherms at −196 °C. Their main textural properties are collected in Table 2. For all catalysts, the specific surface area (S_{BET}) is in the 187–296 $m^2\ g^{-1}$ range. The 1.0P-S16 and 0.5P-S16 catalysts have the largest and lowest S_{BET}, respectively, among the catalysts studied. The N_2 adsorption–desorption isotherms of all sulfided catalysts (not shown here) are of Type IV, with the SBA-15 having a characteristically larger adsorption–desorption hysteresis loop. All isotherms have clear H_1 type hysteresis loops, suggesting that those materials have a very regular mesoporous structure. It is noteworthy that mean pore diameter and pore volume for the SBA-16 are half those of the corresponding SBA-15 materials. As expected from low phosphate content, the textural properties of the phosphate-containing sulfide catalysts are similar to those of their phosphate-free counterparts.

The high-angle XRD technique was used to investigate the presence of any crystallite species in the sulfided catalysts (XRD patterns not shown here). The X-ray patterns of the catalysts show a broad line between 20° and 30°, which is attributed to the amorphous part of the substrates, and the peaks at 2θ (°)= 13.8, 23.3, 33.3, 44.4 and 58.6. Considering our previous study [25,29,30], the peak at 2θ of 23.3° is assigned to β-$CoMoO_4$ crys-

Table 1
Acid properties of the calcined catalysts as determined by TPD-NH_3.

Catalyst	Amount of acid sites (mmol $NH_3\ g_{cat}^{-1}$)			
	Weak T < 250 °C	Moderate T = 250–400 °C	Strong T > 400 °C	Total
0.0P-S15	0.14	0.19	0.58	0.91
0.5P-S15	0.08	0.16	0.41	0.65
1.0P-S15	0.10	0.16	0.46	0.72
0.0P-S16	0.19	0.27	0.45	0.91
0.5P-S16	0.20	0.31	0.52	1.03
1.0P-S16	0.15	0.17	0.35	0.67

Table 2
Textural properties of sulfided catalysts and HRTEM parameters[b] of spent catalysts.

	0.0P-S15	0.5P-S15	1.0P-S15	0.0P-S16	0.5P-S16	1.0P-S16
S_{BET}[a] ($m^2\ g^{-1}$)	223	229	208	208	187	296
V_t[a] ($cm^3\ g^{-1}$)	0.28	0.30	0.29	0.14	0.15	0.22
d[a] (nm)	5.1	5.2	5.5	2.6	3.3	2.9
Average Mo(W)S_2 particle length[b] (nm)	5.1 ± 1.0	4.9 ± 0.9	4.6 ± 1.0	4.7 ± 1.1	5.2 ± 1.0	5.5 ± 1.6
Stacking number[b]	3 ± 1	3 ± 1	3 ± 1	3 ± 1	3 ± 1	3 ± 1
Surface density[b] Mo(W)S_2/50 nm^2	111 ± 23	97 ± 18	97 ± 11	91 ± 27	185 ± 87	111 ± 57

[a] As determined from N_2 adsorption–desorption isotherms at −196 °C for sulfided catalysts; S_{BET}: BET surface area; V_t: total pore volume; d: average pore diameter calculated from the isotherm adsorption branch.
[b] Average length, stacking number and surface density of the Mo(W)S_2 phases as determined by HRTEM.

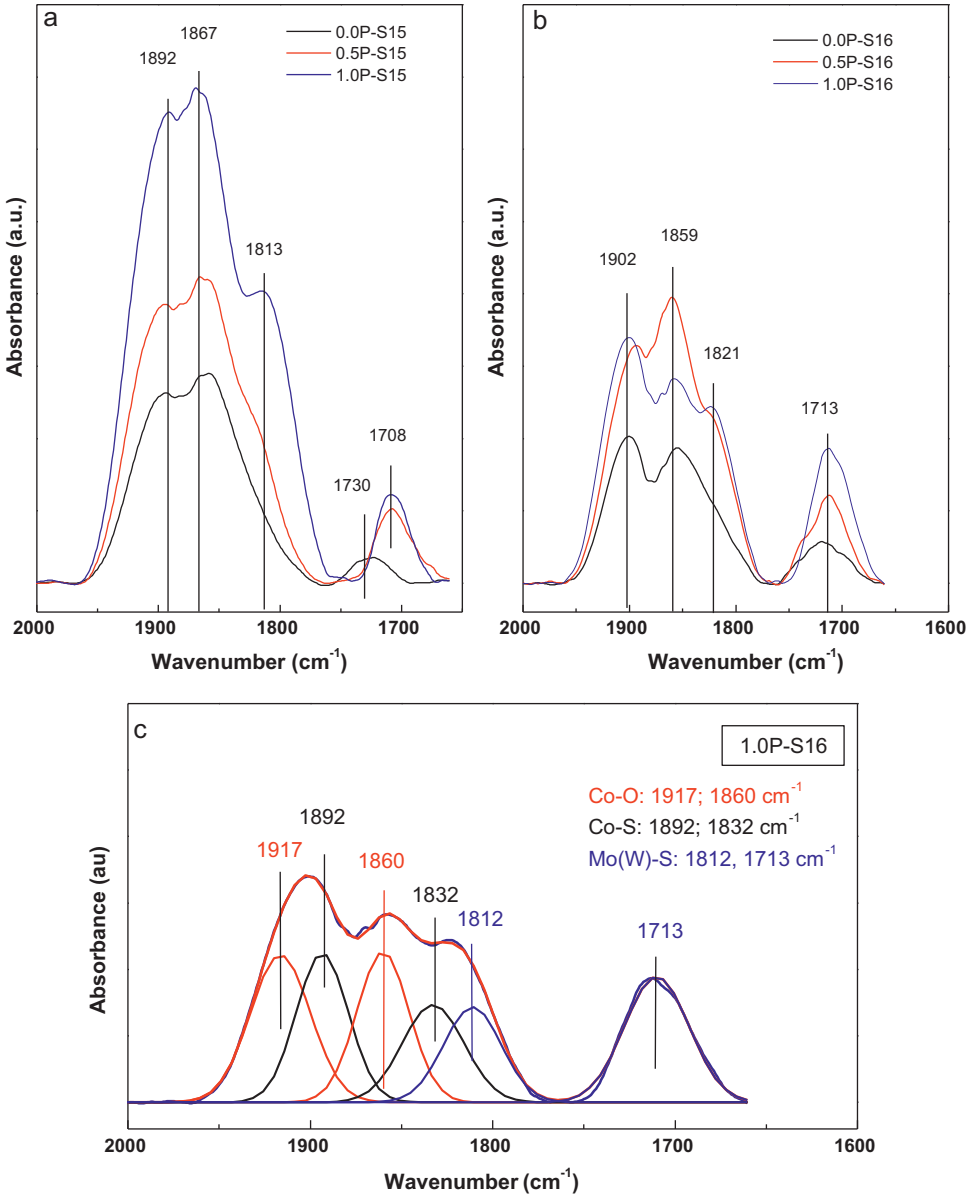

Fig. 1. IR spectra of adsorbed NO at room temperature on sulfided P-free and P-containing CoMoW/SBA-15 (a) and CoMoW/SBA-16 (b) catalysts.

tallites (JCPDS card 21-868). Additionally, the 1.0P-S15 sample shows a peak at $2\theta = 25.9^\circ$ indicative of the formation of the $CoSO_4$ phase (JCPDS card 00-028-0386). The peak at 2θ (°) = 13.8, 44.4 and 58.6 could be assigned to WS_2 (JCPDS card 00-002-0237), whereas the peak at 2θ of 33.3° is probably due to the MoS_2 phase (JCPDS card 01-075-1539). The WS_2 crystal size calculated by the Debye–Scherrer equation for the XRD line at 44.4° follows the trend: 0.5P-S16 = 0.0P-S15 (10.8 nm) < 0.5P-S15 (11.3 nm) < 1.0P-S16 (14.3 nm) < 0.0P-S16 (14.6 nm) < 1.0P-S15 (15.3 nm). Thus, with the exception of 0.5P-S16, the decrease in metal-support interaction due to the presence of phosphate species on the support surface led to the formation of large WS_2 particles. The formation of large metal sulfide species blocking the support pores was also inferred from the N_2 physisorption data (*vide supra*).

DRIFT spectra of NO adsorption at room temperature on SBA-15- and SBA-16 fresh sulfided catalysts are plotted in Fig. 1(a) and (b), respectively. In good agreement with our previous report [28], the SBA-15-based catalysts have bands around 1892, 1867, 1813 and 1708 cm^{-1}, whereas the positions of the bands for the SBA-16-based counterparts were: 1902, 1859, 1821 and 1713 cm^{-1}. The breakdown of those broad bands into Gaussian peaks (Fig. 1(c)) provides three sets of doublets due to the dinitrosyl species on Co^{2+}–O (1917 and 1860 cm^{-1}), Co–S (1892 and 1832 cm^{-1}) and Mo(W)–S (1812 and 1713 cm^{-1}). The bands at 1812 and 1713 cm^{-1} can be assigned to the symmetric and antisymmetric stretching vibrations of NO dimers adsorbed on $Mo(W)S_2$, whereas the doublet bands centered at 1892 and 1832 cm^{-1} can be ascribed to symmetric and antisymmetric stretching vibration modes of NO dimers adsorbed on Co sulfide species, respectively [31–33]. Considering the IR study of NO adsorption on the oxidic form of $CoMo/Al_2O_3$ catalysts [34], the bands at 1917 and 1860 cm^{-1} have a common origin in the symmetric and antisymmetric stretching modes vibration, respectively, of the dinitrosyl species adsorbed on the Co^{2+} ions surrounded by oxide ions. Thus, all catalysts show two types of dinitrosyl species: one adsorbed on Co surrounded by O^{2-} ions and the other one adsorbed on Co^{2+} surrounded by S^{2-} ions. It is commonly accepted that when the "CoMo(W)S" phase is formed, the Co atoms are located at the edge sites of the $Mo(W)S_2$ phases [31–33].

Thus, for both P-free samples, the lowest intensity of their broad band at ca. 1710 cm^{-1} (1730 cm^{-1} for 0.0P-S15) strongly suggests

Table 3
XPS data of the spent catalysts tested in the hydroconversion of anisole[a].

	0.0P-S15	0.5P-S15	1.0P-S15	0.0P-S16	0.5P-S16	1.0P-S16
Co $2p_{3/2}$ (eV)	778.3	778.3	778.3	778.3	778.2	778.2
Mo $3d_{5/2}$ (eV)	229.0	229.0	229.0	229.0	229.0	229.0
W $4f_{7/2}$ (eV)	32.1 (68)	32.1 (74)	32.1 (71)	32.1 (75)	32.2 (85)	32.2 (80)
	33.6 (32)	33.6 (26)	33.6 (29)	33.6 (25)	33.8 (15)	33.8 (20)
Co/Si × 10^3 at	50	38	45	41	39	44
Mo/Si × 10^3 at	11	13	8	9	10	14
W/Si × 10^3 at	8	8	7	9	8	11
$\frac{W-S(32eV)}{W-O(33.7eV)}$ *ratio*	2.1	2.8	2.4	3.0	5.7	4.0
S/(Co + Mo + W) at	1.62	1.81	1.75	1.62	1.59	1.56

[a] C 1s peak at a BE of 284.8 eV was taken as internal reference.

that the edge sites of Mo(W)S_2 particles are covered by Co ions constituting "CoMo(W)S" phases. Therefore, regardless of the type of support, both P-free samples have more Co ions constituting "CoMo(W)S" phases than their P-containing counterparts.

3.3. Characterization of the spent catalysts

The aim of HRTEM measurements was also to compare the morphology of the sulfided phases on the SBA-15 and SBA-16-based spent catalysts (TEM images not shown here). As expected, all spent catalysts present the typical fringes of Mo(W)S_2 crystallites. The arrangement of W(Mo)S_2 layers parallel to the substrate indicates the basal plane attachment. The fact that the particles consist of pure Mo(W)S_2 was confirmed by EDX and by considering the interlayer lattice distance. The slab length, stacking number of Mo(W)S_2 particles and their surface density are compiled in Table 2. As seen in this table, all catalysts record a similar length of Mo(W)S_2 particles and the same number of their stacking layers (3 ± 1 layers). In general, the SBA-16-based systems have higher W(Mo)S_2 slab density than their SBA-15 counterparts, with the 0.5P-S16 sample having the largest population of Mo(W)S_2 crystallites among the catalysts studied. The destruction of the support morphology by produced water did not occur, as it was confirmed by HRTEM of spent catalysts (TEM images not shown here).

Spent catalysts were also studied by X-ray photoelectron spectroscopy. The Si 2p core level peak was close to 103.3 eV for all catalysts, which is characteristic of SiO_2 [35]. The chemical environment of silicon ions was not affected by the presence of other components. As expected, all samples recorded a binding energy of 162.0 eV, which is characteristic of S^{2-} species [26]. The binding energy of the P 2p core-level of the P-containing samples ca. 134.0 eV is indicative of phosphate species [36]. This BE value is much lower than that corresponding to P_2O_5 (135.2 eV), indicating that the phosphorus species remain highly dispersed on the support surface.

Table 3 compiles the binding energy (BE) values corresponding to the W $4f_{7/2}$, Mo $3d_{5/2}$ and Co $2p_{3/2}$ core-levels. As seen in this table, all catalysts record similar BE values, suggesting that the coordination environment for the active sites is similar. The Co $2p_{3/2}$ peak at a binding energy ca. 778.3 eV indicates the formation of a segregated Co_9S_8 phase (BE at 778.4 eV) [37]. Indeed, the difference in binding energies between the Co $2p_{3/2}$ peak and the S 2p peak is 616.4 eV, which is close to the range of 615.7–616.2 eV reported by Alstrup et al. [37] for the Co_9S_8 phase. On the other hand, the Mo $3d_{5/2}$ binding energy at 229.0 eV is characteristic of Mo^{4+} ions in MoS_2 [38]. Contrary to the molybdenum species, the W 4f core level spectra of all spent catalysts has two doublets, each one with the $4f_{7/2}$ and $4f_{5/2}$ components from the spin-orbit splitting (spectra not shown here). The presence of two doublets indicates there are two different W-species. Thus, the W $4f_{7/2}$ core level spectra shows peaks associated with sulfided tungsten species (BE at 32.2 ± 0.1 eV) [39] and oxysulfide W species (BE at 33.7 ± 0.1 eV), which both have a terminal oxygen and a terminal sulfur [40]. It is noteworthy that, in the absence of sulfiding agent in the feed, the partial reduction of metal sulfides upon high hydrogen pressure did not occur. The XPS technique could not detect the W^{3+} species because the W^{3+} ions did not produce a signal that could overcome the more intense WS_2 signal [41]. Considering the percentage of sulfided W species (given in parentheses in Table 3), it appears that the sulfidation degree of the W species in all catalysts was relatively high (68–85%). In addition to the more difficult sulfidation of the W oxide species compared to the Mo oxide, due to differences in the polarization of the metal–oxygen bond [42], the percentage of W sulfide species in the 0.5P-S16 sample was significantly larger than that found for the other catalysts.

The distribution of supported Co, Mo and W species was estimated by comparing Co/Si, W/Si and Mo/Si atomic intensity ratios (Table 3). In general, all catalysts have a very similar surface exposure of the Co, Mo and W species. Noticeably, the surface exposure of Mo and W is much lower than that of the Co promoter, suggesting the location of Mo and W species within the inner support porous structure and the main location of Co species on the outer support surface.

3.4. Catalytic activity in anisole hydrotreating

The time-on-stream behavior of SBA-15- and SBA-16-based catalysts in the anisole hydroconversion reaction is shown in Fig. 2(a) and (b), respectively. As seen, all catalysts deactivate during the first 3 h of on-stream operation, with the 0.5P-S16 sample being the most stable among the catalysts studied. The steady-state conversion data are listed in Table 4. According to this table, the activity of the catalysts follows the trend: 0.5P-S16 > 0.0P-S15(16) ≈ 1.0P-S15 > 0.5P-S15 > 1.0P-S16. Thus, contrary to the SBA-15 substrate, the presence of a small amount of phosphate (0.5 wt%) on the surface of the SBA-16 substrate has a positive effect for the catalytic response of the 0.5P-S16 sample. Both P-free SBA-15(16)-based catalysts have similar activities, indicating that support morphology is not the principal factor influencing the catalytic behavior of those materials.

In a fixed bed high-pressure flow reactor and under operating conditions ($T = 310\,^{\circ}C$, $P = 3$ MPa, $WHSV = 24.5\ h^{-1}$), the products identified by GC were phenol, *o*-cresol, methylanisole, *o*-xylenol and benzene. A study of the selectivity at an anisole conversion of 38% reveals almost the same selectivity for all catalysts studied (Table 4). An analysis of selectivity results suggests that two independent reaction paths are operative in anisole transformation over CoMoW/SBA-15(16) catalysts: demethylation of anisole and methyl transfer to benzene ring (see reaction Scheme 1). The former reaction route led to the formation of phenol (selectivity in the 60.6–65.9% range), whereas the latter led to the formation of *o*-cresol and *o*-xylenol (selectivity in the 22.0–25.9% and 8.4–11.2% ranges, respectively). Thus, anisole transformation over

Table 4
Activity, selectivity[a] and catalyst deactivation in the hydrotreating of anisole (T = 310 °C, P = 3.0 MPa, $WHSV$ = 24.5 h^{-1}) over sulfided CoMoW/(x)P/SBA-15(16) catalysts.

	0.0P-S15	0.5P-S15	1.0P-S15	0.0P-S16	0.5P-S16	1.0P-S16
Conversion at 4 h (%)	27.5	22.1	27.5	24.3	35.2	11.8
Phenol[a] (%)	60.1	60.6	62.7	60.8	61.1	65.9
o-Cresol[a] (%)	25.9	25.4	24.4	25.1	25.0	22.0
o-Xylenol[a] (%)	11.2	10.8	10.7	10.8	10.7	8.4
o-Methylanisole[a] (%)	1.7	1.3	1.7	1.8	1.9	2.3
Benzene[a] (%)	1.0	1.9	0.5	1.5	1.4	1.4
Deactiv.[b] (%)	44.4	43.2	38.2	39.7	18.9	72.4
Coke[c] (wt%)	1.9	1.2	28.0	2.2	0.2	0.7
SO_2[c] (%)	1.3	2.2	17.1	4.4	0.3	0.4

[a] At anisole conversion of 38%.
[b] As calculated from Eq. (2).
[c] As determined from the spent catalysts weights losses during by TPO/TGA experiments.

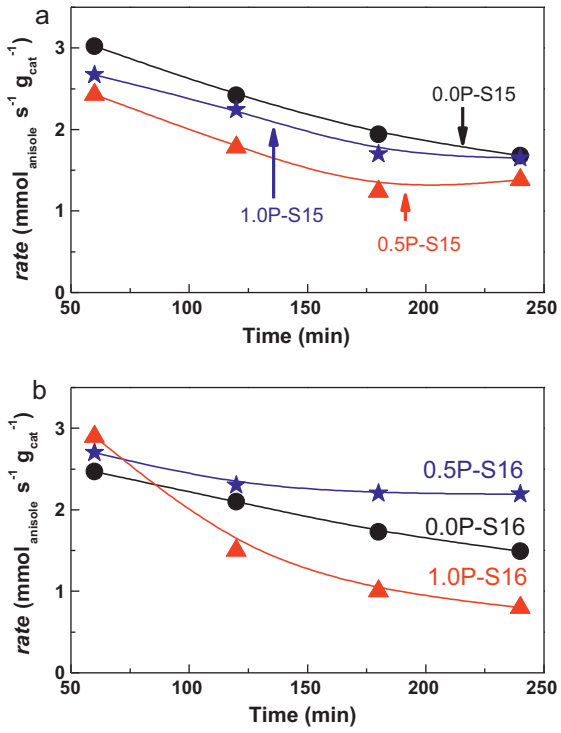

Fig. 2. Time-on-stream behavior of sulfided SBA-15-based (a) and SBA-16-based catalysts (b) in the hydroconversion of anisole at T = 310 °C, P = 3 MPa and $WHSV$ = 24.5 h^{-1}.

sulfide CoMoW/SBA-15(16) catalysts occurs mainly via the cleavage of the alicyclic carbon and oxygen bond, with phenol being the main reaction product. The direct hydrogenolysis of phenol (HDO selectivity) led to the formation of benzene, although deoxygenation over all catalysts was not significant (selectivity ca. 2%). As expected, the direct splitting of the methoxy group of anisole did not occur because the bond between the alicyclic carbon and oxygen is weaker than the bond between the aromatic carbon and oxygen [15]. This is consistent with the literature [15], even though the catalysts and/or reaction conditions were different. For example, the reported selectivity in the gas phase hydrodeoxygenation of anisole when the commercial sulfided Co–Mo catalysts (Albemarle Co.) were used under mild conditions (T = 300 °C, P = 1.0 MPa) was: 41% phenol, ca. 30% methylphenols isomers, 23% benzene and 5% cyclohexane [15], and the results are fairly consistent with those in this study.

Concerning catalyst stability during on-stream conditions, a common practice for maintaining the catalyst activity in HDO on sulfided catalysts involves the addition of a sulfiding agent (H_2S or CS_2). However, this practice does not avoid the deactivation of the sulfided Co–Mo/γ-Al_2O_3 catalysts [15,43]. In this study, the sulfiding agent was not added to the feed mixture because our objective was to study the effect of acidity on the catalyst performance, which could be masked by H_2S addition because–SH groups formed on the support surface could be involved in the HDO reaction [20]. Moreover, the competitive adsorption of the S-containing compound and anisole on the same active sites (sulfur adsorbs on CUS sites and affects the reactions occurring on these sites) is expected to be avoided without masking the catalyst sensitivity toward deactivation by water (H_2S might to compensate the inhibition by water produced during HDO reaction [44]). Concerning the possible lost of active sites due to transformation of the metal sulfides into metals,

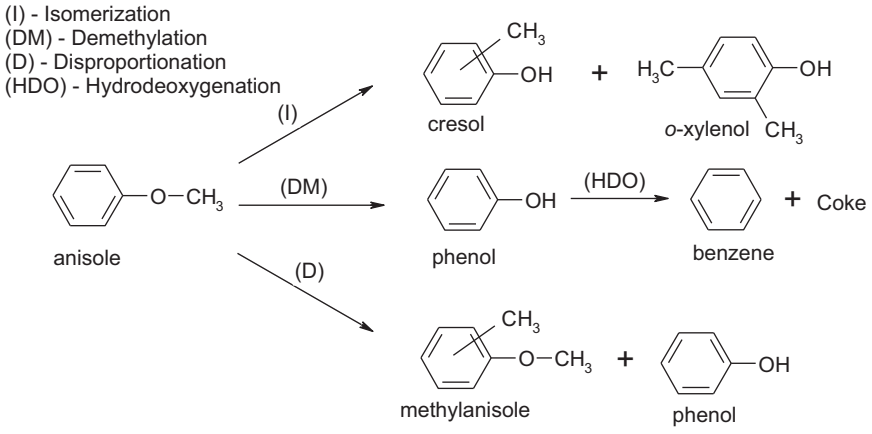

Scheme 1. Scheme of the anisole HDO reaction over CoMoW/(x)P/SBA-15(16) catalysts (x = 0.0, 0.5, 1.0 wt% of P).

the XPS measurements of the spent catalysts did not reveal formation of metal phases upon reaction conditions employed (*vide supra*).

The percentage of catalyst deactivation calculated from Eq. (2) is listed in Table 4. As seen in this table, the most active 0.5P-S16 catalyst recorded the lowest deactivation among the catalysts studied. Since the HDO reaction paths depend heavily on the state of the catalyst surface during on-stream reaction [45], the catalyst's coking behavior was evaluated from the weight change of the coked catalysts during temperature-programmed oxidation (TPO), followed by the TG-DTG technique (TGA profiles not shown here). As expected, all catalysts recorded a weight loss at ca. 400 °C ascribed to the loss of sulfur atoms from the oxysulfide species and a second weight loss corresponding to the DTG peak centered at ca. 600 °C, which was due to coke oxidation [46]. The amounts of coke and SO_2 formed (as determined by catalyst weight loss at about 400 and 600 °C, respectively) are listed in Table 4. As seen in this table, the most active 0.5P-S16 shows the lowest deactivation during on-stream reaction (18.9%) linked with absence of coke formation (0.2%) and the largest stability of metal sulfide phases. On the contrary, the 1.0P-S15 sample showed the lowest stability of their metal sulfide phases and the largest deactivation due to coke formation (Table 4). With exception of this sample, coke reactions in all catalysts were negligible (0.2–1.9%), suggesting that neither the catalyst morphology nor the presence of a small amount of phosphate on the support surface influenced coke formation. This might explain the similar selectivities recorded in the HDO of anisole over all catalysts.

In short, it is shown that sulfided CoMoW catalysts supported on both SBA-15 and SBA-16 record moderate activity for removing oxygen from bio-liquids and, on the other hand, they are interesting catalysts for isomerization reactions. For all catalysts, coke formation was much lower than expected from the activity decay during the first 4 h of on-stream operation (Table 4), indicating that other factors than coke formation might contribute to the decrease in catalyst activity. This point has been discussed below.

4. Catalyst activity–structure correlation

Considering the similar or even larger average length of Mo(W)S_2 phase (from HRTEM) with respect to catalyst pore diameter (Table 2), it is clear that active phases in all catalysts studied are located on the support surface. Such location is even more evident in the case of SBA-16-based catalysts. From the catalyst activity–structure correlation, the best catalytic response of the sulfided 0.5P-S16 sample in the hydroconversion of anisole could be explained by considering a combination of various effects. The first is the largest surface exposure of the active phases, as determined by HRTEM, presenting active phases homogeneously dispersed on both internal and external catalyst surfaces. Moreover, the 0.5-PS16 catalyst records the largest total acidity among the catalysts studied (Table 1). Considering a correlation between the strong acid sites of the oxide precursors (from TPD-NH_3) and steady-state catalytic activity (see Fig. 3(a)), the major activity of this sample could be explained by considering that the cleavage of the methyl carbon–oxygen bond might take place on both metal sulfides and on acidic sites of the support, as proposed by Huuska et al. [12,13]. In such a case, one might assume that a homolytic splitting of the methyl carbon–oxygen bond might occur on the metal sulfides followed by a rapid hydrogenation of the radicals formed, whereas a dominating reaction of heterolytic scission might occur on the acidic sites of the support. If so, the methyl carbonium ion formed would attack the aromatic ring. Since those ions possess a non-planar adsorption state, the attack occurs preferentially in the ortho position [12].

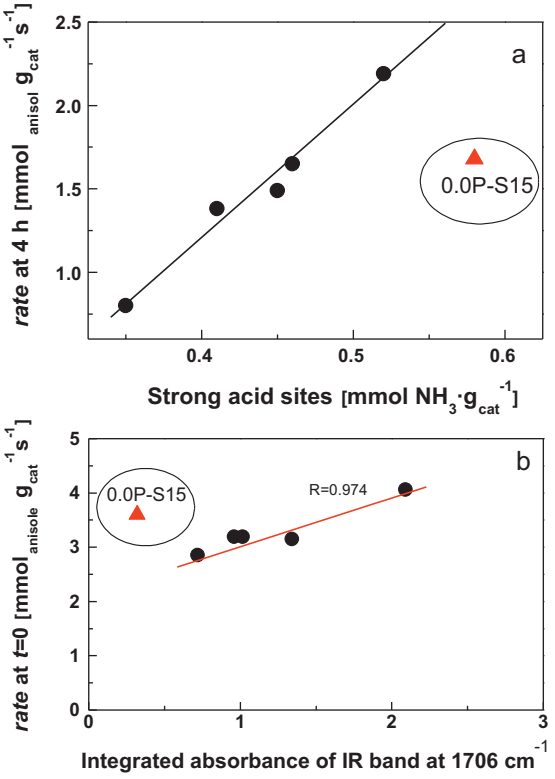

Fig. 3. (a) Correlation between the strong acid sites of the oxide precursors (from TPD-NH_3) and steady-state catalytic activity. (b) Correlation between the number of "CoMo(W)S" sites of the sulfided catalysts (from DRIFT-NO) and initial catalytic activity.

All catalysts record both low selectivity toward benzene and the non-hydrogenation of the aromatic ring, suggesting the absence of the metallic-like so-called brim sites, which were recently shown to be involved in hydrogenation reactions [17–19]. Moreover, a large selectivity toward isomerization products confirms the hypothesis that the HDO reaction requires two types of active sites: one for the activation of dihydrogen, with the other being a metal oxide with a variable oxidation state (support) for the activation of oxy-groups [18]. We found a correlation between the number of "CoMo(W)S" sites, as determined by integrated absorbance of the IR band at ca. 1710 cm^{-1} (measured by nitric oxide adsorption at room temperature on sulfided catalysts), and initial catalytic activity, suggesting that those types of active sites are formed during catalyst sulfidation (see Fig. 3(b)). However, this phase is not stable during on-stream operation, as confirmed by the XPS of spent catalysts. This might partially explain the activity decay during the first 4 h of on-stream reaction (Table 4). Another factor which could contribute to catalyst deactivation is the partial reduction of metal sulfides under high hydrogen pressure. However, the XPS measurements of spent catalysts preclude this possibility. Since water is always present in the reactor during HDO reaction, it is more likely that adsorption of H_2O molecules on the active sites contributes to catalyst deactivation [44]. The largest stability of the 0.5P-S16 sample during on-stream reaction indicated that modification of SBA-16 material with small amount of phosphate (0.5 wt%) prevent catalyst deactivation by water and coke, the latter confirmed by TPO-TGA measurement.

Thus, in the worst scenario of absence of sulfiding agent, the most active 0.5P-S16 catalyst showed a good stability during on-stream HDO reaction indicating that the catalyst deactivation by coke and water can be diminished by appropriate modification of the surface chemistry of the SBA-16 support with optimized

amount of phosphate. Our previous study on the upgrading of olive oil production-derived by-products via hydrotreating on sulfided CoMo/SBA-15(16) mesoporous silica demonstrated that those catalysts were more active than a commercial $NiMo/Al_2O_3$ catalyst [6]. Interestingly, considering the formation of desirable products (paraffins and alcohols) and the removal of oxygen-containing products and polyaromatics, the SBA-16-based catalyst was found to be more appropriate for upgrading of bio-liquid than its SBA-15 counterpart. Contrary to the binary CoMo/SBA-15(16) systems studied previously [6], the ternary CoMoW/SBA-15(16) catalysts tested in the HDO of model feed exhibited a low selectivity toward O-free products indicating that their hydrogenolysis capability needs to be improved for the HDO of pyrolysis oils.

5. Conclusions

SBA-15- and SBA-16-supported Co–Mo–W catalysts were evaluated for the hydroconversion of anisole in a fixed bed catalytic high-pressure flow reactor ($T = 310\,^{\circ}C$, $P = 3$ MPa, $WHSV = 24.5\ h^{-1}$). The mechanism of anisole transformation over SBA-15(16)-based sulfide Co–Mo–W catalysts was bifunctional, with the acidic function being larger than the metallic one, as deduced from the promotion of the isomerization pathway and the non-hydrogenation of the aromatic ring. The HRTEM results suggest that the SBA-16 support favors the dispersion of metallic sulfides more than its SBA-15 counterpart. It was found that catalyst deactivation by coke and water can be diminished by appropriate modification of the surface chemistry of the SBA-16 support with optimized amount of phosphate. The largest activity of Co–Mo–W/SBA-16 modified with 0.5 wt% of phosphate appears to be linked to its largest population of active sites, highest total acidity and best stability during on-stream conditions. In the worst scenario of absence of sulfiding agent, this sample exhibited a good stability and resistance to deactivation by coke and water. However, the low selectivity toward O-free products indicates that the hydrogenolysis capability of Co–Mo–W/SBA-16 catalysts needs to be improved for the HDO of pyrolysis oils.

Acknowledgement

Financial support by the Spanish Ministry of Science and Innovation (Project ENE2007-67533-C02-01) and Comunidad de Madrid (S2009ENE-1743) is gratefully acknowledged. The authors acknowledge the assistance of Dr. M.A. Peña in TPO/TG measurements.

References

[1] A.V. Bridgwater, D. Meier, D. Radlein, Org. Geochem. 30 (1999) 1479–1493.
[2] D.C. Elliott, Energy Fuels 12 (2007) 1792–1815.
[3] E. Furimsky, Appl. Catal. A: Gen. 199 (2000) 147–190.
[4] E.G. Baker, D.C. Elliott, C. Duglas, UK Patent 5180868 (1993).
[5] E. Laurent, A. Centeno, B. Delmon, 6th Proc. Inter Symp. Catalyst Deactivation, Stud. Surf. Sci. Catal. 88 (1994) 573–578.
[6] R. Nava, B. Pawelec, P. Castaño, M.C. Álvarez-Galván, C.V. Loricera, J.L.G. Fierro, Appl. Catal. B: Environ. 92 (2009) 154–167.
[7] A. Centeno, E. Laurent, B. Delmon, J. Catal. 154 (1995) 288–298.
[8] M. Ferrari, S. Bosmans, R. Maggi, B. Delmon, P. Grange, Catal. Today 65 (2001) 257–264.
[9] M. Ferrari, B. Delmon, P. Grange, Carbon 40 (2002) 497–511.
[10] S. Echeandia, P.L. Arias, V.L. Barrio, B. Pawelec, J.L.G. Fierro, Appl. Catal. B: Environ. 101 (2010) 1–12.
[11] J. B-son Bredenberg, M. Huuska, J. Räty, M. Korpio, J. Catal. 77 (1982) 242–247.
[12] M. Huuska, J. Rintala, J. Catal. 94 (1985) 230–238.
[13] M.K. Huuska, Polyhedron 5 (1986) 233–236.
[14] T.-R. Viljava, E.R.M. Saari, A.O.I. Krause, Appl. Catal. A: Gen. 209 (2001) 33–43.
[15] V.A. Yakovlev, S.A. Khromova, O.V. Sherstyuk, V.O. Dundich, D.Yu. Ermakov, V.M. Novopashina, M.Yu. Lebedev, O. Bulavchenko, V.N. Parmon, Catal. Today 144 (2009) 362–366.
[16] B. Pawelec, J.M. Campos-Martin, E. Cano-Serrano, R.M. Navarro, S. Thomas, J.L.G. Fierro, Environ. Sci. Technol. 39 (2005) 3374–3381.
[17] H. Topsøe, B. Hinnemann, J.K. Nørskov, J.V. Lauritsen, F. Besenbacher, P.L. Hansen, G. Hytoft, R.G. Egeberg, K.G. Knudsen, Catal. Today 107–108 (2005) 12–22.
[18] B. Hinnemann, J.K. Nørskov, H. Topsøe, J. Phys. Chem. B 109 (2005) 2245–2253.
[19] Á. Logadóttir, P.G. Moses, B. Hinnemann, N.-Y. Topsøe, K.G. Knudsen, H. Topsøe, J.K. Nørskov, Catal. Today 111 (2006) 44–51.
[20] A.Y. Bunch, X. Wang, U.S. Ozkan, J. Mol. Catal. 270 (2007) 264–272.
[21] A.Y. Bunch, X. Wang, U.S. Ozkan, J. Catal. 206 (2002) 177–187.
[22] D. Zhao, J. Feng, Q. Huo, N. Melosh, G.H. Fredrickson, B.F. Chmelka, G.D. Stucky, Science 279 (1998) 548–552.
[23] W.J.J. Stevens, K. Lebeau, M. Mertens, G. Van Tendeloo, P. Cool, E.F. Vansant, J. Phys. Chem. B 110 (2006) 9183–9187.
[24] K. Flodström, V. Alfredsson, Microporous Mesoporous Mater. 59 (2003) 167–176.
[25] R. Nava, R.A. Ortega, G. Alonso, C. Ornelas, B. Pawelec, J.L.G. Fierro, Catal. Today 127 (2007) 70–84.
[26] A. Stanislaus, M. Absi-Halabi, K.Al. -Dolama, Appl. Catal. 39 (1988) 239–253.
[27] N. Spanos, A. Lycourghiotis, J. Colloid Interface Sci. 171 (1995) 306.
[28] W.C. Cheng, N.P. Luthra, J. Catal. 109 (1988) 163–169.
[29] R. Nava, B. Pawelec, J. Morales, R.A. Ortega, J.L.G. Fierro, Microporous Mesoporous Mater. 118 (2009) 189–201.
[30] R. Nava, J. Morales, G. Alonso, C. Ornelas, B. Pawelec, J.L.G. Fierro, Appl. Catal. A: Gen. 321 (2007) 58–70.
[31] N.Y. Topsøe, H. Topsøe, J. Catal. 77 (1982) 293–296.
[32] N.Y. Topsøe, H. Topsøe, J. Catal. 84 (1983) 386–401.
[33] J.L.G. Fierro (Ed.), Spectroscopic Characterization of Heterogeneous Catalysts, Part B, Elsevier Science Publishers, Amsterdam, 1990, p. B67.
[34] C.V. Caceres, J.L.G. Fierro, M.N. Blanco, H.J. Thomas, Appl. Catal. 10 (1984) 333–346.
[35] D. Briggs, M.P. Seah (Eds.), Practical Surface Analysis. Auger and X-ray Photoelectron Spectroscopy, Wiley, New York, Salle and Sauerländer, 1990.
[36] B. Pawelec, D. Damyanova, R. Mariscal, J.L.G. Fierro, I. Sobrados, J. Sanz, L. Petrov, J. Catal. 223 (2004) 86–97.
[37] Ib Alstrup, Ib Chorkendorff, R. Candia, B.S. Clausen, H. Topsøe, J. Catal. 77 (1982) 397–409.
[38] G. de la Puente, A. Gil, J.J. Pis, P. Grange, Langmuir 15 (1999) 5800–5806.
[39] B. Pawelec, R. Navarro, J.L.G. Fierro, P.T. Vasudevan, Appl. Catal A: Gen. 168 (1998) 205–217.
[40] A.P. Shpak, A.M. Korduban, L.M. Kulikov, T.V. Kryshchuk, N.B. Konig, V.O. Kandyba, J. Electron Spectrosc. Relat. Phenom. 181 (2010) 234–238.
[41] K.T. Nag, D.M. Hercules, J. Phys. Chem. 80 (1976) 2094–2102.
[42] J.P. Mangnus, B. Scheffer, J.A. Moulijn, Am. Chem. Soc. Petrol. Div. Prepar. 32 (1987) 329.
[43] O.İ. Şenol, T.-R. Viljava, A.O.I. Krause, Appl. Catal. A: Gen. 326 (2007) 236–244.
[44] O.İ. Şenol, T.-R. Vijava, A.O.I. Krause, Catal. Today 106 (2005) 186–189.
[45] E.O. Odebunmi, D.F. Ollis, J. Catal. 80 (1983) 56–64.
[46] R. Huirache-Acuña, B. Pawelec, E. Rivera-Muñoz, R. Nava, J. Espino, J.L.G. Fierro, Appl. Catal. B: Environ. 92 (2009) 168–184.